

# The 2006 Radio Outburst of a Microquasar Cyg X-3: Observation and Data

M. TSUBOI, T. TOSAKI, N. KUNO, K. NAKANISHI, T. SAWADA, T. UMEMOTO  
*Nobeyama Radio Observatory\*, Minamimaki, Minamisaku, Nagano, 384-1305*

S. A. TRUSHKIN

*Special Astrophysical Observatory RAS, Nizhnij Arkhyz, Karachaevo-Cherkassia 369167, Russia*

T. KOTANI, N. KAWAI

*Tokyo Tech, 2-12-1 O-okayama, Meguro, Tokyo 152-8551*

Y. KURONO, T. HANDA, K. KOHNO

*Institute of Astronomy, The University of Tokyo, Mitaka, Tokyo 181-0015*

T. TSUKAGOSHI

*The Graduate University for Advanced Studies, 2-21-1 Osawa, Mitaka, Tokyo 181-0015*

O. KAMEYA, H. KOBAYASHI

*Mizusawa VERA Observatory, Mizusawa, Oshu, Iwate 023-0861*

K. FUJISAWA, A. DOI

*Faculty of Science, Yamaguchi University, Yamaguchi, Yamaguchi 753-8512*

T. OMODAKA

*Faculty of Science, Kagoshima University, Kagoshima, Kagoshima 890-0065*

H. TAKABA, H. SUDOU, K. WAKAMATSU

*Faculty of Engineering, Gifu University, Gifu 501-1193*

Y. KOYAMA, E. KAWAI

*National Institute of Information and Communications Technology, Kashima, Ibaraki 314-8501*

and

N. MOCHIZUKI, Y. MURATA

*Institute of Space and Astronautical Science, Sagamihara, Kanagawa 229-8510*

(Received Mar. 31, 2007; accepted Oct. 10, 2007, PASJ)

## Abstract

We present the results of the multi-frequency observations of radio outburst of the microquasar Cyg X-3 in February and March 2006 with the Nobeyama 45-m telescope, the Nobeyama Millimeter Array, and the Yamaguchi 32-m telescope. Since the prediction of a flare by RATAN-600, the source has been monitored from Jan 27 (UT) with these radio telescopes. At the eighteenth day after the quench of the activity, successive flares exceeding 1 Jy were observed successfully. The time scale of the variability in the active phase is presumably shorter in higher frequency bands.

We also present the result of a follow-up VLBI observation at 8.4 GHz with the Japanese VLBI Network (JVN) 2.6 days after the first rise. The VLBI image exhibits a single core with a size of  $< 8$  mas (80 AU). The observed image was almost stable, although the core showed rapid variation in flux density. No jet structure was seen at a sensitivity of  $T_b = 7.5 \times 10^5$  K.

**Key words:** black hole physics — stars: variables: other — radio continuum: stars

## 1. Introduction

Cyg X-3 is a famous X-ray binary including a black hole candidate (e.g., Schalinski et al. 1998). This object is classified as a microquasar due to its bipolar relativistic jet accompanied by radio flares. Because it is located on the Galactic plane at a distance of about 10 kpc (e.g., Predehl et al. 2000) and obscured by intervening interstellar matter, it has been observed mainly in radio and X-ray. Its giant radio flares have been observed once every several years since its initial discovery (Gregory et al. 1972; Braes & Miley 1972). The peak flux densities in the radio flares have often increased up to levels of 10 Jy or more at centimeter wave (e.g., Waltman et al. 1994). The radio emission seems to be correlated with hard X-ray emission, and not with soft X-ray emission (McCullough et al. 1999). Although the radio emission arises through synchrotron process of relativistic electrons in the jet (Hjellming & Johnston 1988), the millimeter behavior during the flares is not yet established. An observation at a shorter wavelength and with a higher time resolution is desirable to understand the mechanism of the flares.

The quenched state of Cyg X-3, in which the radio emission is suppressed below 1 mJy, is a possible precursor of flares (e.g., Waltman et al. 1994). In January 2006, this quenched state was detected in monitoring observations with the RATAN-600 radio telescope (Trushkin et al. 2006). The source has been monitored from MJD= 53762 (Jan 27 2006 in UT) with the Nobeyama 45-m radio telescope (NRO45), the Nobeyama Millimeter Array (NMA), and the Yamaguchi 32-m radio telescope (YT32). We detected the initial state, or rising phase, of the radio flare of Cyg X-3 at MJD= 53768 (February 2 2006) and observed successive flares exceeding 1 Jy (Tsuboi et al. 2006), which turned out to be the beginning of an active phase lasting more than 40 days .

In this paper, radio observations with NRO45, NMA, YT32, and the Japanese VLBI Network (JVN) are reported. The observation procedures are summarized in section 2. The light curves and the spectral evolution observed with NRO45, NMA and YT32 are shown in

---

\* The Nobeyama Radio Observatory is a branch of the National Astronomical Observatory, National Institutes of Natural Sciences, Japan.

section 3, together with the result of JVN. Detailed discussion based on these observations will be published as separate papers.

## 2. Observations and data reductions

### 2.1. Radio photometric observations

The first observation period was from MJD= 53763.13 (January 28 2006) to 53779.94 (February 13 2006). Observations with NRO45 of Cyg X-3 were performed alternately at 23 GHz and at both 43 and 86 GHz, simultaneously. The period corresponded to the initial phase of the radio flaring state in February-March 2006. The second period was from MJD= 53805.12 (2006 March 11) to 53808.77 (2006 March 14). A cooled HEMT receiver with dual circular polarization feed was used at 23 GHz. SIS receivers with orthogonal linear polarization feeds were used at 43 and 86 GHz. The system noise temperatures during the observations, including atmospheric effects and antenna ohmic loss, were 80–120 K at 23 GHz, 120–200 K at 43 GHz, and 250–350 K at 86 GHz. The full width at half maximums (FWHM) of the telescope beams are 77'' at 23 GHz, 39'' at 43 GHz, and 19'' at 86 GHz. The telescope beam was alternated between the positions of the source and sky at 15 Hz by the beam-switch in order to subtract atmospheric effect. Antenna temperatures were calibrated by the chopper wheel method. The primary flux calibrator for conversion from antenna temperature to flux density was a proto-planetary nebula, NGC 7027, whose flux density values are given as 5.5 Jy at 23 GHz, 5.0 Jy at 43 GHz, and 4.6 Jy at 86 GHz (Ott et al. 1994). Telescope pointing was checked and corrected in every observation procedure by observing NGC 7027 in cross-scan mode. The pointing accuracy was better than 3'' r.m.s. during these observations. The source was observed using ON-OFF observations of durations of 5–10 minutes, sufficient to detect and perform photometry on Cyg X-3 and the calibrator.

Interferometric observations were performed with the NMA from MJD= 53762.18 (January 27 2006) to 53776.15 (February 10 2006) at both 98 and 110 GHz simultaneously. The NMA consists of six 10m antennas equipped with cooled DSB SIS receivers with a single linear polarization feed. The Ultra-Wide-Band Correlator with a 1GHz bandwidth was employed for the backend (Okumura et al. 2000). The quasar 2017+370 was used as a phase and amplitude reference calibrator and Uranus and Neptune were used as primary flux-scale calibrators. The system noise temperatures during the observations, including atmospheric effects and antenna ohmic loss, were 80–120 K at 98 GHz and 120–200 K at 110 GHz. The uv-data were calibrated with the UVPROC-II software package developed at NRO (Tsutsumi, Morita, & Umeyama 1997), and then imaged with natural UV weighting, and CLEANed with the NRAO AIPS package.

Centimeter-wave observations of Cyg X-3 were also performed at 8.4 GHz for longer duration with YT32. The observation period was from MJD= 53768.29 (February 2 2006)

to 53813.08 (March 19 2006). A cooled HEMT receiver was used at 8.4 GHz. The system noise temperature of YT32 during the observations, including atmospheric effects and antenna ohmic loss, was 45 K at 8.4 GHz. The primary flux calibrator for YT32 was an H II region, DR21 with a flux density of 20 Jy at 8.4 GHz. Flux measurement was carried out with ON-OFF switching method with an overlaying small-angle offset for both azimuth and elevation directions. Additional observations using YT32 were also performed in May 2006. Data at MJD= 53872 was obtained with the Mizusawa VERA Observatory 10-m radio telescope.

The uncertainty in flux density of Cyg X-3 depends on weather conditions. However, sensitivity of telescopes is not the principal factor of the uncertainty. Because the primary flux-scale calibrator for NRO45, NGC 7027, is close to Cyg X-3 in the celestial sphere, the difference of atmospheric attenuation between these sources has no significant effect on the data. The typical systematic uncertainty is  $\sim 10\%$  for NRO45. The typical systematic uncertainty of NMA is  $\sim 15\%$  because the primary flux-scale calibrators are not near to Cyg X-3 and phase noise caused by atmospheric fluctuations. Although flux loss due to pointing errors is corrected by pointing offset data in the data reduction process, the uncertainty of YT32 is as much as  $\sim 20\%$ . However, the relative uncertainties of flux density in a day should be much better than these values.

## 2.2. JVN observation

A follow-up VLBI observation was carried out with the Japanese VLBI Network (JVN; Fujisawa et al. 2007; Doi et al. 2006a; Doi et al. 2006b). The duration of the observation was from MJD= 53770.8 to MJD= 53771.4, i.e., starting 2.6 days after the first rise of the flare. The telescopes participating in this observation are four 20-m telescopes of the VLBI Exploration of Radio Astrometry project (VERA; Kobayashi et al. 2003), Usuda 64-m (U64), Kashima 34-m (K34), YT32, and Gifu 11-m (G11). Right-circular polarization was received at 8400–8416 MHz (IF1) and 8432–8448 MHz (IF2) with a total bandwidth of 32 MHz. The VSOP/K4-terminal system was used as a digital back-end; digitized data in 2-bit quantization are recorded onto magnetic tapes at a data rate of 128 Mbps. Two sources (2000+472, 3C454.3) other than Cyg X-3 were observed for gain and bandpass calibration, respectively. The data were correlated with the VSOP-FX correlator at NAOJ (Shibata et al. 1998), and fringe were detected at all baselines except for baselines including Ishigaki, Ogasawara, and G11 telescopes.

The data was reduced in the standard manner with the Astronomical Image Processing System (AIPS; Greisen 2003) developed at the US National Radio Astronomy Observatory. An amplitude-scaling factor was determined from monitored system noise temperatures and antenna efficiencies of U64, YT32, and K34 telescopes. Furthermore, we calibrated antenna gain variations using the data of 2000+472, which is a point source in the JVN baselines and scanned every 30–60 minutes. Such a calibration method provides an absolute flux scale with an accuracy of  $\sim 10\%$  and a relative time variation of antenna gain of  $\sim 3\%$  accuracy.

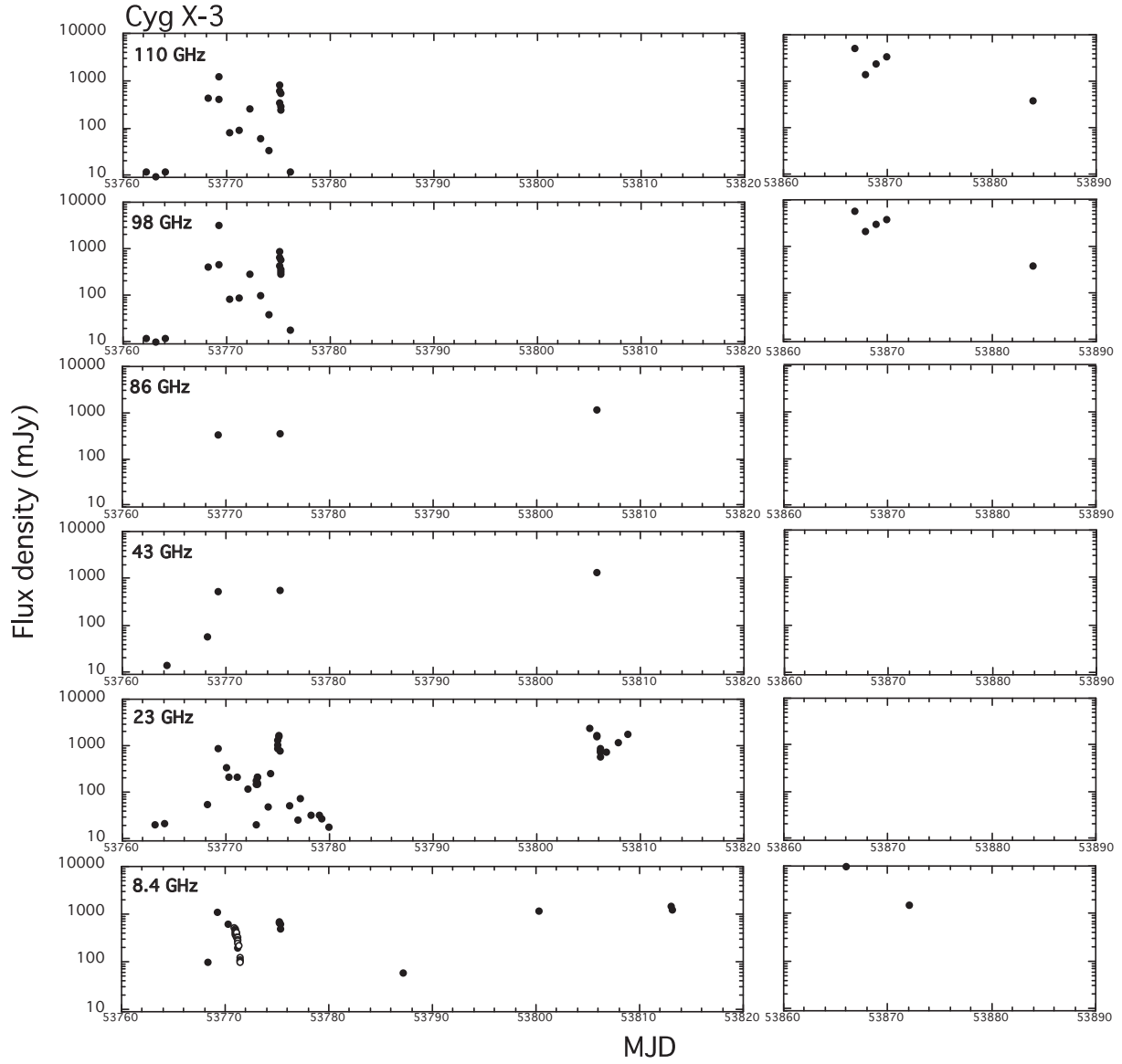
### 3. Results

#### 3.1. Light curves

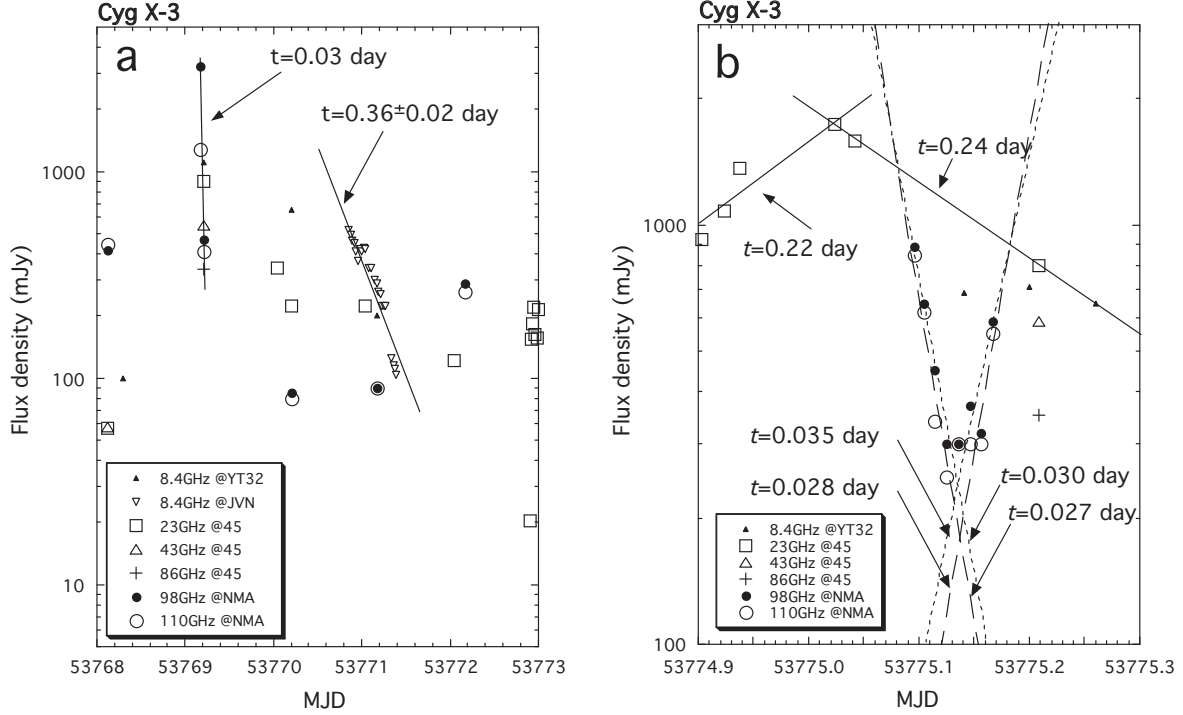
We present the light curves of Cyg X-3 at 6 frequency bands of 8.4, 23, 43, 86, 98, and 110 GHz obtained with NRO45, NMA, and YT32 in Fig. 1. Table 1 summarizes results of observations. The first rise of the flare was detected with NMA at MJD= 53768.13 or 3 am on February 2 2006 (UT) at 98 and 110 GHz. This is about 18 days after it entered the quenched state observed with RATAN-600. The first rise was also observed at lower frequencies within 1 day. After that, we observed several peaks exceeding 1 Jy. Although there is a long intermission of observation in our campaign, the duration of the active phase of Cyg X-3 is at least over 40 days (Tosaki et al. 2006). It can be confirmed that Cyg X-3 was still active in May from the flux densities at 8.4, 98, and 110 GHz in 2006 May in Fig. 1 and Table 1.

Figure 2a shows the enlarged light curves of the initial phase of the first flare. Before the flare, the flux density of Cyg X-3 was inhibited up to a few 10 mJy at 23 to 110 GHz (see Figure 1). At MJD= 53768.13, the first rise was found by NMA at 98 and 110 GHz, of which the flux densities became 40 times or more compared with the value of the previous day. The flux densities at 23 and 43 GHz with NRO45 were also 3-4 times brighter than the previous values. The peak flux densities at MJD= 53769.17 exceed 3 Jy at 98 GHz and 1 Jy at 110 GHz. They were violently variable and decreased to 1 Jy or less within one hour. Assuming an exponential decay, the e-folding decay times would be 0.03 days both at 98 GHz and 110 GHz. On the other hand, the e-folding decay time at 8.4 GHz are  $t = 0.36 \pm 0.02$  day during MJD= 53770 to 53771, which will be mentioned for details. For several major flares of Cyg X-3 observed previously, the e-folding decay time of the flux density was reported to be in the range of 0.15 to 2.75 days (Hjellming et al. 1974). The observed decay times are much shorter than these previous values.

Figure 2b shows the enlarged light curves of the second flare. We obtained a higher sampling rate light curve at 23 GHz in the rising phase of the second flare. At MJD= 53774.9, the rise of the second flare was detected at 23 GHz with the NRO45. The flux density at 23 GHz increased rapidly from 0.9 to 1.7 Jy within 3 hours. That corresponds to an e-folding rise time of  $t = 0.22 \pm 0.05$  day. The flux density decreased rapidly from the peak to 0.8 Jy by the next observation 4.4 hours after. If these flux densities are involved in the same flare, the e-folding decay time is  $t = 0.24 \pm 0.01$  day. The decay phase of the flare was also observed at other frequencies. The flux densities observed at 98 and 110 GHz decreased rapidly within the observation interval as at 23 GHz. A power law describes the decay behavior. The e-folding decay times at 98 and 110 GHz are  $t = 0.030 \pm 0.003$  day and  $t = 0.027 \pm 0.005$  day, respectively. These are of the same order of the first flare at 98 and 110 GHz. In addition to the peak and following decay at 23 GHz, another rising is recognized at 98 and 110 GHz in the observation break at 23 GHz. The e-folding rise times at 98 and 110 GHz are  $t = 0.035 \pm 0.025$  day and



**Fig. 1.** Radio light curves of February to May 2006 of Cygnus X-3 at, from bottom to top, 8.4, 23, 43, 86, 98, and 110 GHz. The 8.4 GHz data were obtained with YT32. In addition, open circles at 8.4 GHz show high-density sampling flux densities observed by the Japanese VLBI Network (JVN). The 23, 43 and 86 GHz data were obtained with NRO45. The 98 and 110 GHz data were obtained with NMA. The first rise was detected at MJD= 53768.13 at 98 and 110 GHz. Within one day after the first rise, the flux density at 23 GHz also increased. The 8.4, 98, and 110 GHz data show Cyg X-3 was in an active phase in May 2006.



**Fig. 2.** Enlarged radio light curves of Cyg X-3 at the first and second flares. **(a)** Observation epoch is from MJD = 53768 to 53773. At MJD= 53768.13, the first rise was found by NMA at 98 and 110 GHz, and the flux densities increased up to 0.4 Jy. This is 40 times or more compared with the value before the first rise. The flux densities at MJD= 53769.17 exceed 3 Jy at 98 GHz and 1 Jy at 110 GHz. They decreased to 1 Jy or less within one hour. The best-fitting curves of exponential decay model are plotted in lines. Open upside-down triangles show flux densities at 8.4 GHz observed by the Japanese VLBI Network (JVN). The flux densities at lower frequencies changed more gradually. **(b)** Observation epoch is from MJD = 53774.9 to 53775.3. Data with NMA at 98 and 110 GHz show clearly the quench and the successive rapid rise of the millimeter flux. The best-fit curves of exponential rise and decay models are plotted in lines. The e-folding rise and decay times are  $t \simeq 0.03$  day both at 98 and 110 GHz.

$t = 0.028 \pm 0.013$  day, respectively. The e-folding rise times are also at the same level as the decay times.

Figure 3 shows the relation between the time scale of the flux variability and frequency in the 2006 flares of Cyg X-3. The e-folding rise and decay times are derived from neighboring observations within 8 hours. Our data with higher sampling rates than previous reports should reveal new information about the synchrotron jets of Cyg X-3. The e-folding time is shorter at higher frequencies, and we fit the trend with a power-law model, shown as a straight line in the figure. Although the scattering of the data points is large, the e-folding time is inversely proportional to the observed frequency,  $T = 3.8f^{-1.03}$ . That cannot be explained in terms of the synchrotron bubble model, which predicts the same time scale for all the frequencies. It is suggested that the injection and loss of energy of relativistic electrons in the jet plays an important role in the spectral evolution of the flares of Cyg X-3.



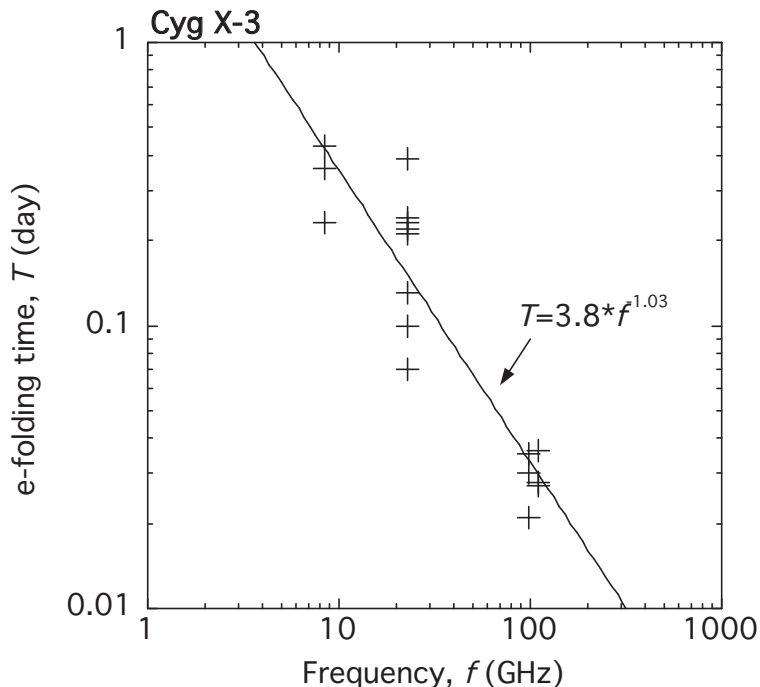
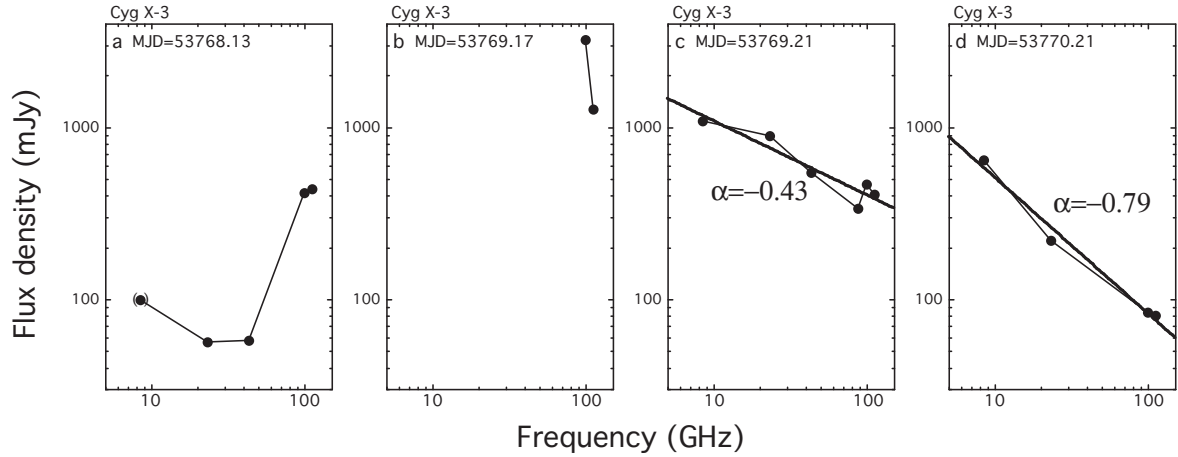


**Fig. 3.** The relation between the time scale of the flux variability and frequency in the 2006 flares of Cyg X-3. The solid line is the best-fitting power-law model for these data. The e-folding time of the flux variability should inversely relate frequency.

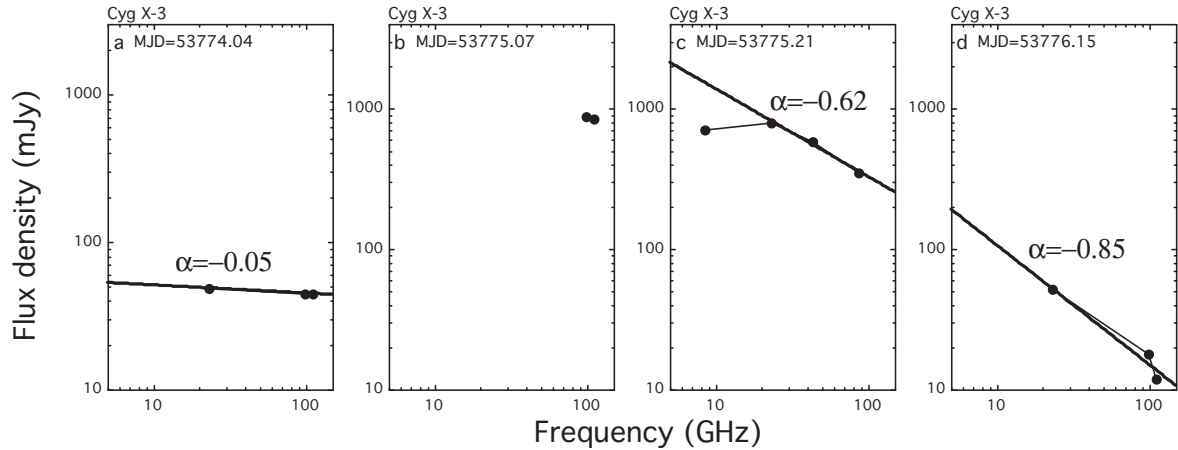
### 3.2. Spectral Evolution of Flares

Fig. 4 shows spectral evolution in the three days around the first flare of Cyg X-3. The curve in panel **a** indicates the spectrum at MJD= 53768.13, at the onset of the first flare. The rapid increase at 98 and 110 GHz takes place first as mentioned in the previous subsection, while the flux densities at lower frequencies do not change significantly. The spectrum shows a complicated inverted feature from 43 to 98 GHz. This suggests there is time lag of flare onset depending on frequency. The data in panel **b** indicate flux densities at 98 and 110 GHz at MJD= 53769.17. The flux densities at 98 GHz and 110 GHz rise to 3.2 and 1.3 Jy, respectively. These are the highest values in this flare. Unfortunately, no simultaneous data at other frequencies are available. Panel **c** shows the flux densities of Cyg X-3 at MJD= 53769.21, just after 1 hour of panel **b**. The flux densities at lower frequencies increased about 10 times over values in panel **a**, but flux densities at 98 and 110 GHz decreased dramatically in 1 hour. Then the spectrum is described by a power law with an index of  $\alpha \simeq -0.4$ . The peak flux is followed by a rapid decay at high frequency. Panel **d** shows the spectrum at MJD= 53770.21, or 1 day after the peak. The spectrum is also describable by a power law, but it was decayed to be as steep as  $\alpha \simeq -0.8$ . This is consistent with the decay time being shorter at higher frequency, as mentioned in the previous subsection. We assume that the spectral break seen at  $\sim 100$  GHz at MJD= 53768.13 moves in the spectrum down to below 8 GHz in one day. This evolution of the radio spectrum may be interpreted as the result of an adiabatic expansion of





**Fig. 4.** Spectral evolution during the first flare. Three days evolution around the first peak at MJD= 53768. **a** On the first day at the first flare, MJD= 53768.14, the flux densities at 98 and 110 GHz increase rapidly, while the flux densities at lower frequencies were still low. **b** 98 and 110 GHz data at MJD= 53769.17. The flux densities at 98 GHz and 110 GHz were 3.2 and 1.3 Jy, respectively. These are the highest values in this flare. Unfortunately, it was not observed during this time at other frequencies. **c** Flux densities after 1 hour of panel **b**. The flux densities at 8.4, 22, and 43 GHz increased about 10 times over values in panel **a**. Flux densities at 98 and 110 GHz decreased dramatically in 1 hour. A power-law model,  $S \propto f^\alpha$ , is applied to these (solid line). The best fitting of the spectral index is  $\alpha \simeq -0.4$ . **d** Flux densities after 1 day of panel **c**. Although the flux densities were described by a power law (solid line), the spectrum was fairly steepened. The best fitting of the spectral index is  $\alpha \simeq -0.8$ .



**Fig. 5.** Three days spectral evolution during the second flare around MJD= 53775. **a** Flux densities one day before the second flare, or at MJD= 53774.04. The flux densities were described by a power law with  $\alpha \simeq -0.1$  (solid line). **b** Flux densities at MJD= 53775.07. These are the highest values at 98 and 110 GHz in this flare. They would be near the peak of this flare because the highest value appeared at 22 GHz before 1 hour. Unfortunately, it was not observed during this time at 98 and 110 GHz. **c** Flux densities after 3 hour of panel **b**, Between these two panels, Cyg X-3 decreased and increased rapidly. (see also Fig 2b). Flux densities except for at 8.4 GHz were described by a power law with  $\alpha \simeq -0.6$  (solid line). **d** Flux densities after 1 day of panel **c**. The spectrum was steepened. The best fitting of the spectral index is  $\alpha \simeq -0.8$ .

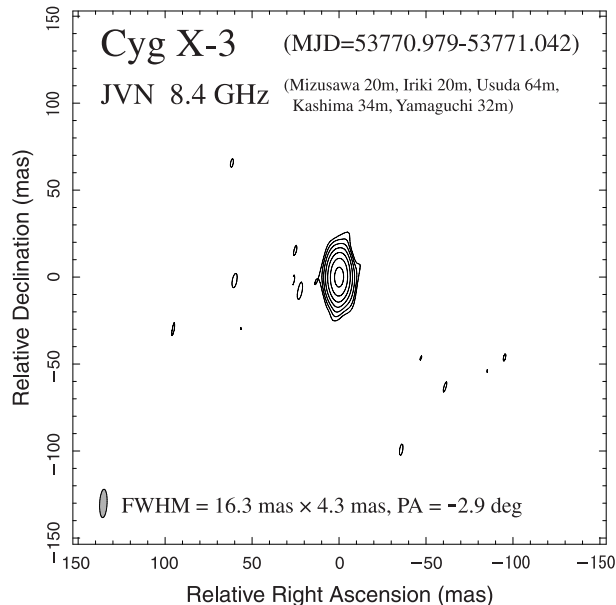
synchrotron emitting ejecta in Cyg X-3.

Figure 5 shows the spectral evolution in the three days around the second flare. Panel **a** in this figure indicates spectra on the day before the second peak or at MJD= 53774.04. This shows a flat spectrum with an index of  $-0.1$ , which suggests that the second flare has already started. The spectrum at another flare in March was also flat over the observation band, suggesting an optically thick radio source. A power law with an index of  $-0.2$  can explain the spectrum. Panel **b** shows flux densities at MJD= 53775.07. These are the highest values at 98 and 110 GHz in this flare. Following this, these decreased rapidly. However, they would be near the peak of this flare, because the value at 22 GHz reached the maximum before 1 hour. Unfortunately, it was not observed during this time at 98 and 110 GHz. Panel **c** shows flux densities after 3 hour of panel **b**, Between these two panels, Cyg X-3 decreased and increased rapidly. (see also Fig 2b). Flux densities except for at 8.4 GHz were described by a power law with  $\alpha \simeq -0.6$  (solid line). The spectral index is slightly steeper than that in the corresponding phase of the first flare. And panel **d** shows flux densities after 1 day of panel **c**. The spectrum was steepened. The best fitting of the spectral index is  $\alpha \simeq -0.9$ . The spectral index of  $-0.9$  is similar to that one day after the first flare. The decay time of the second flare is also shorter at higher frequencies, which cannot be explained by the sole synchrotron bubble model.

### 3.3. 8.4 GHz VLBI results in a flare

Our VLBI observation started from just 2 days after the first rise of the flare, i.e., the first day after the intensity maximum of the first flare. Successive snapshots with a short integration time have been made because rapid flux decrease has also been observed during the VLBI observation. Fig. 6 is an example of such a snapshot, of which observation period is from MJD= 53770.979 to 53771.042. Only a featureless (extended) structure is found in all snapshot images. Deconvolution with the structure model of an elliptical Gaussian profile and self-calibration was done using DIFMAP software (Shepherd 1997). The deconvolved source size was  $\sim 8$  mas. This is significantly broader than a synthesized beam size,  $16.3 \text{ mas} \times 4.3 \text{ mas}$  at PA of  $-2.9^\circ$ . However, no other component is found beyond three times the r.m.s. of noise of the resultant image or a brightness temperature of  $7.5 \times 10^5$  K.

We also analyzed the time evolution of flux density and source structure during the JVN observation. We have clipped out a series of data segments. Each segment has a duration of 1 hour, and the interval of the starting time of the segments is set to be 0.5 hour, i.e., half of a duration overlapping the half of the next duration. Using the task of UVFIT in AIPS, we measured a source size and a flux density for each clipped data by visibility-based model-fitting using an elliptical Gaussian profile model. The flux density of the component decreased from  $\sim 500$  mJy to  $\sim 100$  mJy during the VLBI observation lasting  $\sim 14$  hours (Fig.2a and Fig 7a). The source structure has hardly changed, regardless of the variability of the synthesized beam (Fig.7b and 7c). The weighted averages of major axis, minor axis, and position angles of the



**Fig. 6.** Snapshot image of Cyg X-3 from VLBI data in MJD = 53770.979 to 53771.042 (1.5 hour). The beam size is  $16.3 \text{ mas} \times 4.3 \text{ mas}$  at PA of  $-2.9^\circ$ , corresponding to  $157 \text{ AU} \times 41 \text{ AU}$  at the distance to Cyg X-3. R.M.S. of image noise,  $\sigma$ , is  $0.70 \text{ mJy beam}^{-1}$ . Contour levels are  $3\sigma \times (-1, 1, 2, 4, 8, 16, 32, 64)$ .

source structure are  $8.9 \pm 0.1 \text{ mas}$ ,  $7.1 \pm 0.1 \text{ mas}$ , and  $15.0 \pm 2.3 \text{ deg}$ , respectively, i.e., we have resolved the source which is slightly but significantly elongated in a north-south direction. Our VLBI observation has revealed that Cyg X-3 has no significant structure change in spite of the rapid flux variability at 8.4 GHz during the period.

Previous studies (Miller-Jones et al. 2004) show that the two-sided jets are ejected toward north and south after major radio flares. If the ejection was concurrent with the first rise of the flux and the jet axis is fairly close to perpendicular to the line of sight, the traveling distance of the ejecta is expected to be 350 AU or 35 mas at 10 kpc. However, we have not found any evidence of such a jet structure. The source size in our VLBI image is presumably affected by interstellar scattering because it is consistent with the expected scattering size at 8.4 GHz (Schalinski et al. 1995). Thus, there is no structural evolution on a scale of larger than 5 mas in spite of rapid flux variability. That may be a strong constraint on jet evolution in a few days after a radio flare.

The authors would like to thank the members of NRO45 group and NMA group of Nobeyama Radio Observatory for support in the observations. This work is partially supported by the Japan-Russia Research Cooperative Program of Japan Society for the Promotion of Science. The studies are partially supported by the Russian Foundation Base Research (RFBR) grant N 05-02-17556 and the mutual RFBR and Japan Society for the Promotion of Science (JSPS) grant N 05-02-19710. The JVN project is led by the National Astronomical Observatory of Japan (NAOJ) that is a branch of the National Institutes of

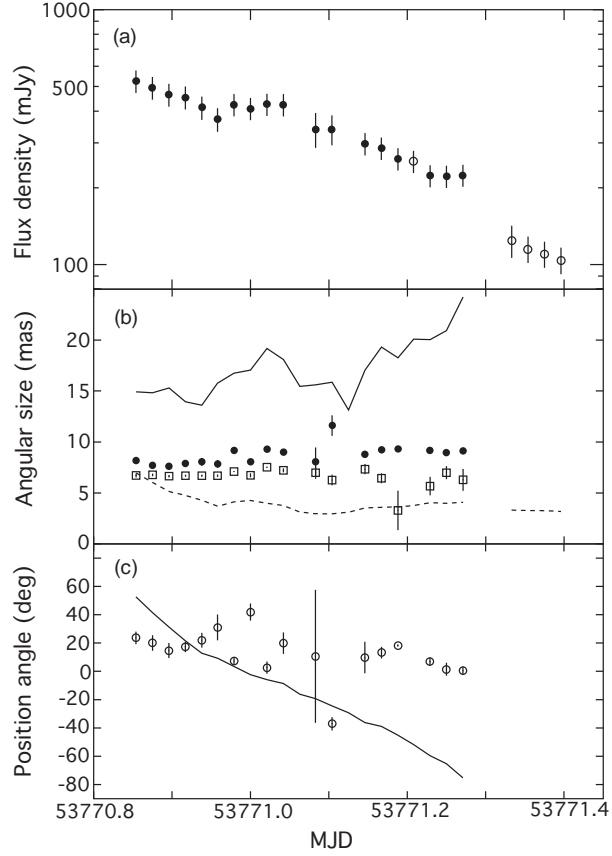


**Fig. 7.** Evolution of source structure of Cyg X-3 obtained with VLBI. A series of measurements were performed by visibility-based model-fitting using an elliptical-Gaussian profile model with free parameters of flux density, major and minor axes of FWHM, and position angle of the major axis (see text in detail). **(a)** Flux densities of VLBI component (filled circle). Open circles represent measurements using a circular-Gaussian model, rather than elliptical one, due to poor data quality. **(b)** Angular sizes of fitted source structure. Filled circles and open squares represent the FWHMs of major and minor axes, respectively. Solid and dashed lines represent the major and minor axes of HPBWs of synthesized beam in uniform-weighting, for comparison. **(c)** Position angles of major axis of fitted source structure (open circle). Solid line represents the position angle of the major axis of synthesized beam, for comparison.

Natural Sciences (NINS), Hokkaido University, Gifu University, Yamaguchi University, and Kagoshima University, in cooperation with the Geographical Survey Institute (GSI), the Japan Aerospace Exploration Agency (JAXA), and the National Institute of Information and Communications Technology (NICT). TK is supported by a 21st Century COE Program at Tokyo Tech “Nanometer-Scale Quantum Physics” by the Ministry of Education, Culture, Sports, Science and Technology.

## References

- Braes, L. L. E., & Miley, G. K. 1972, *Nature*, 237, 506
- Doi, A., et al. 2006a, astro-ph/0612528
- Doi, A., et al. 2006b, *PASJ*, 58, 777
- Fujisawa, K., et al. 2007, in prep.
- Gregory, P. C., Kronberg, P. P., Seaquist, E. R., Hughes, V., A., Woodsworth, A., Viner, M. R., & Retallack, D. 1972, *Nature*, 239, 440
- Hjellming, R. M., Brown, R. L., & Blankenship, L. C. 1974, *ApJ*, 194, L13
- Hjellming, R. M., & Johnston, K. J. 1988, *ApJ*, 328, 600
- Kobayashi, H., et al. 2003, *Astronomical Society of the Pacific Conference Series*, 306, 367
- Greisen, E. W. 2003, *Information Handling in Astronomy - Historical Vistas*, 109
- McCullough, M. L., Robinson, C. R., Zhang, S. N., Harmon, B. A., Hjellming, R. M., Waltman, E. B., Foster, R. S., Ghigo, F. D., Briggs, M. S., Pendleton, G. N., & Johnston, K. J. 1999, *ApJ*, 517, 951
- Miller-Jones, J. C. A., Blundell, K. M., Rupen, M. P., Mioduszewski, A. J., Duffy, P., & Beasley, A. J. 2004, *ApJ*, 600, 368
- Okumura, S. K., Momose, M., Kawaguchi, N. et al., 2000, *PASJ*, 52, 393
- Ott, M., Witzel, A., Quirrenbach, A., et al., 1994, *A&A* 284, 331
- Predehl, P., Bruwitz, V., Paerels, F., & Trümper, J. 2000, *A&A*, 357, L25
- Schalinski, C. J., et al. 1995, *ApJ*, 447, 752
- Schalinski, C. J., Johnston, K. J., Witzel, A., Waltman, E. B., Umana, G., Pavelin, P. E., Ghigo, F. D., Venturi, T., Mantovani, F., Foley, A. R., Spencer, R. E., & Davis, R. J. 1998, *A&A*, 329, 504
- Shepherd, M. C. 1997, *ASP Conf. Ser. 125: Astronomical Data Analysis Software and Systems VI*, 125, 77
- Shibata, K. M., Kameno, S., Inoue, M., & Kobayashi, H. 1998, *ASP Conf. Ser. 144: IAU Colloq. 164: Radio Emission from Galactic and Extragalactic Compact Sources*, 144, 413
- Trushkin, S. A., Nizhelskij, N. A., Bursov, N. N., & Majorova, E. K. 2006, in *IAU Symp. 238*, 166
- Tsuboi, M. et al. 2006, *ATel*, 727, 1
- Tosaki, T., Tsuboi, M., Nakanishi, K., Trushkin, S., Fujisawa, K., Kameya, O., Kotani, T., & Kawai, N. 2006, *ATel*, 952, 1
- Tsutsumi, T., Morita, K.-I., & Umeyama, S. 1997, in *ASP Conf. Ser. 125, Astronomical Data Analysis Software and Systems VI*, ed. G. Hunt & H. E. Payne (San Francisco: ASP), 50

Waltman, E. B., Fiedler, R. L., Johnston, K. L., & Ghigo, F. D. 1994, AJ, 108, 179

**Table 1.** Flux densities of Cyg X-3

MJD	$S_{8.4}$ GHz	$S_{23}$ GHz	$S_{43}$ GHz	$S_{86}$ GHz	$S_{98}$ GHz	$S_{110}$ GHz
[day]	[mJy]	[mJy]	[mJy]	[mJy]	[mJy]	[mJy]
53762.181					12	12
53763.125		20			10	9.6
53764.083		21			12	12
53764.208			15			
53768.125		57	58		417	442
53768.292	100					
53769.167					3247	1280
53769.208	1100	896	549	338	468	408
53770.042		339				
53770.208	650	222			85	80
53771.042		224				
53771.167	200				89	90
53772.042		122				
53772.167					288	260
53772.910		20				
53772.924		155				
53772.934		183				
53772.951		219				
53772.965		163				
53772.982		156				
53772.995		214				
53773.208					104	60
53774.042		49			39	35
53774.208		255				
53774.903		922				
53774.924		1080				
53774.937		1365				
53775.024		1732				
53775.042		1589				
53775.096					890	850
53775.104					650	620
53775.115					450	340
53775.125					300	250
53775.135					300	300



Table 1. (Continued.)

MJD [ <i>day</i> ]	$S_{8.4}$ GHz [ <i>mJy</i> ]	$S_{23}$ GHz [ <i>mJy</i> ]	$S_{43}$ GHz [ <i>mJy</i> ]	$S_{86}$ GHz [ <i>mJy</i> ]	$S_{98}$ GHz [ <i>mJy</i> ]	$S_{110}$ GHz [ <i>mJy</i> ]
53775.140	690					
53775.146					370	300
53775.156					320	300
53775.167					590	550
53775.200	710					
53775.208		801	587	352		
53775.260	650					
53775.320	500					
53776.152		52			18	12
53776.958		25				
53777.188		74				
53778.208		33				
53778.948		34				
53779.208		29				
53779.937		18				
53787.125	60					
53800.208	1200					
53805.118		2424				
53805.729		1762				
53805.750		1609				
53805.757			1402	1203		
53806.090		805				
53806.104		896				
53806.118		733				
53806.139		601				
53806.708		764				
53807.771		1192				
53808.771		1782				
53813.000	1530					
53813.083	1260					
53866.014	10000					
53866.847					6000	5200
53867.847					2200	1400
53868.847					3000	2500
53869.847					3900	3500

Table 1. (Continued.)

MJD	$S_{8.4}$ GHz	$S_{23}$ GHz	$S_{43}$ GHz	$S_{86}$ GHz	$S_{98}$ GHz	$S_{110}$ GHz
[ <i>day</i> ]	[ <i>mJy</i> ]	[ <i>mJy</i> ]	[ <i>mJy</i> ]	[ <i>mJy</i> ]	[ <i>mJy</i> ]	[ <i>mJy</i> ]
53872.014	1500					
53883.847					400	400

# The 2006 Radio Outburst of a Microquasar Cyg X-3: Observation and Data

M. TSUBOI, T. TOSAKI, N. KUNO, K. NAKANISHI, T. SAWADA, T. UMEMOTO  
*Nobeyama Radio Observatory\*, Minamimaki, Minamisaku, Nagano, 384-1305*

S. A. TRUSHKIN

*Special Astrophysical Observatory RAS, Nizhnij Arkhyz, Karachaevo-Cherkassia 369167, Russia*

T. KOTANI, N. KAWAI

*Tokyo Tech, 2-12-1 O-okayama, Meguro, Tokyo 152-8551*

Y. KURONO, T. HANDA, K. KOHNO

*Institute of Astronomy, The University of Tokyo, Mitaka, Tokyo 181-0015*

T. TSUKAGOSHI

*The Graduate University for Advanced Studies, 2-21-1 Osawa, Mitaka, Tokyo 181-0015*

O. KAMEYA, H. KOBAYASHI

*Mizusawa VERA Observatory, Mizusawa, Oshu, Iwate 023-0861*

K. FUJISAWA, A. DOI

*Faculty of Science, Yamaguchi University, Yamaguchi, Yamaguchi 753-8512*

T. OMODAKA

*Faculty of Science, Kagoshima University, Kagoshima, Kagoshima 890-0065*

H. TAKABA, H. SUDOU, K. WAKAMATSU

*Faculty of Engineering, Gifu University, Gifu 501-1193*

Y. KOYAMA, E. KAWAI

*National Institute of Information and Communications Technology, Kashima, Ibaraki 314-8501*

and

N. MOCHIZUKI, Y. MURATA

*Institute of Space and Astronautical Science, Sagamihara, Kanagawa 229-8510*

(Received Mar. 31, 2007; accepted Oct. 10, 2007, PASJ)

## Abstract

We present the results of the multi-frequency observations of radio outburst of the microquasar Cyg X-3 in February and March 2006 with the Nobeyama 45-m telescope, the Nobeyama Millimeter Array, and the Yamaguchi 32-m telescope. Since the prediction of a flare by RATAN-600, the source has been monitored from Jan 27 (UT) with these radio telescopes. At the eighteenth day after the quench of the activity, successive flares exceeding 1 Jy were observed successfully. The time scale of the variability in the active phase is presumably shorter in higher frequency bands.

We also present the result of a follow-up VLBI observation at 8.4 GHz with the Japanese VLBI Network (JVN) 2.6 days after the first rise. The VLBI image exhibits a single core with a size of  $< 8$  mas (80 AU). The observed image was almost stable, although the core showed rapid variation in flux density. No jet structure was seen at a sensitivity of  $T_b = 7.5 \times 10^5$  K.

**Key words:** black hole physics — stars: variables: other — radio continuum: stars

## 1. Introduction

Cyg X-3 is a famous X-ray binary including a black hole candidate (e.g., Schalinski et al. 1998). This object is classified as a microquasar due to its bipolar relativistic jet accompanied by radio flares. Because it is located on the Galactic plane at a distance of about 10 kpc (e.g., Predehl et al. 2000) and obscured by intervening interstellar matter, it has been observed mainly in radio and X-ray. Its giant radio flares have been observed once every several years since its initial discovery (Gregory et al. 1972; Braes & Miley 1972). The peak flux densities in the radio flares have often increased up to levels of 10 Jy or more at centimeter wave (e.g., Waltman et al. 1994). The radio emission seems to be correlated with hard X-ray emission, and not with soft X-ray emission (McCullough et al. 1999). Although the radio emission arises through synchrotron process of relativistic electrons in the jet (Hjellming & Johnston 1988), the millimeter behavior during the flares is not yet established. An observation at a shorter wavelength and with a higher time resolution is desirable to understand the mechanism of the flares.

The quenched state of Cyg X-3, in which the radio emission is suppressed below 1 mJy, is a possible precursor of flares (e.g., Waltman et al. 1994). In January 2006, this quenched state was detected in monitoring observations with the RATAN-600 radio telescope (Trushkin et al. 2006). The source has been monitored from MJD= 53762 (Jan 27 2006 in UT) with the Nobeyama 45-m radio telescope (NRO45), the Nobeyama Millimeter Array (NMA), and the Yamaguchi 32-m radio telescope (YT32). We detected the initial state, or rising phase, of the radio flare of Cyg X-3 at MJD= 53768 (February 2 2006) and observed successive flares exceeding 1 Jy (Tsuboi et al. 2006), which turned out to be the beginning of an active phase lasting more than 40 days .

In this paper, radio observations with NRO45, NMA, YT32, and the Japanese VLBI Network (JVN) are reported. The observation procedures are summarized in section 2. The light curves and the spectral evolution observed with NRO45, NMA and YT32 are shown in

---

\* The Nobeyama Radio Observatory is a branch of the National Astronomical Observatory, National Institutes of Natural Sciences, Japan.

section 3, together with the result of JVN. Detailed discussion based on these observations will be published as separate papers.

## 2. Observations and data reductions

### 2.1. Radio photometric observations

The first observation period was from MJD= 53763.13 (January 28 2006) to 53779.94 (February 13 2006). Observations with NRO45 of Cyg X-3 were performed alternately at 23 GHz and at both 43 and 86 GHz, simultaneously. The period corresponded to the initial phase of the radio flaring state in February-March 2006. The second period was from MJD= 53805.12 (2006 March 11) to 53808.77 (2006 March 14). A cooled HEMT receiver with dual circular polarization feed was used at 23 GHz. SIS receivers with orthogonal linear polarization feeds were used at 43 and 86 GHz. The system noise temperatures during the observations, including atmospheric effects and antenna ohmic loss, were 80–120 K at 23 GHz, 120–200 K at 43 GHz, and 250–350 K at 86 GHz. The full width at half maximums (FWHM) of the telescope beams are 77'' at 23 GHz, 39'' at 43 GHz, and 19'' at 86 GHz. The telescope beam was alternated between the positions of the source and sky at 15 Hz by the beam-switch in order to subtract atmospheric effect. Antenna temperatures were calibrated by the chopper wheel method. The primary flux calibrator for conversion from antenna temperature to flux density was a proto-planetary nebula, NGC 7027, whose flux density values are given as 5.5 Jy at 23 GHz, 5.0 Jy at 43 GHz, and 4.6 Jy at 86 GHz (Ott et al. 1994). Telescope pointing was checked and corrected in every observation procedure by observing NGC 7027 in cross-scan mode. The pointing accuracy was better than 3'' r.m.s. during these observations. The source was observed using ON-OFF observations of durations of 5–10 minutes, sufficient to detect and perform photometry on Cyg X-3 and the calibrator.

Interferometric observations were performed with the NMA from MJD= 53762.18 (January 27 2006) to 53776.15 (February 10 2006) at both 98 and 110 GHz simultaneously. The NMA consists of six 10m antennas equipped with cooled DSB SIS receivers with a single linear polarization feed. The Ultra-Wide-Band Correlator with a 1GHz bandwidth was employed for the backend (Okumura et al. 2000). The quasar 2017+370 was used as a phase and amplitude reference calibrator and Uranus and Neptune were used as primary flux-scale calibrators. The system noise temperatures during the observations, including atmospheric effects and antenna ohmic loss, were 80–120 K at 98 GHz and 120–200 K at 110 GHz. The uv-data were calibrated with the UVPROC-II software package developed at NRO (Tsutsumi, Morita, & Umeyama 1997), and then imaged with natural UV weighting, and CLEANed with the NRAO AIPS package.

Centimeter-wave observations of Cyg X-3 were also performed at 8.4 GHz for longer duration with YT32. The observation period was from MJD= 53768.29 (February 2 2006)

to 53813.08 (March 19 2006). A cooled HEMT receiver was used at 8.4 GHz. The system noise temperature of YT32 during the observations, including atmospheric effects and antenna ohmic loss, was 45 K at 8.4 GHz. The primary flux calibrator for YT32 was an H II region, DR21 with a flux density of 20 Jy at 8.4 GHz. Flux measurement was carried out with ON-OFF switching method with an overlaying small-angle offset for both azimuth and elevation directions. Additional observations using YT32 were also performed in May 2006. Data at MJD= 53872 was obtained with the Mizusawa VERA Observatory 10-m radio telescope.

The uncertainty in flux density of Cyg X-3 depends on weather conditions. However, sensitivity of telescopes is not the principal factor of the uncertainty. Because the primary flux-scale calibrator for NRO45, NGC 7027, is close to Cyg X-3 in the celestial sphere, the difference of atmospheric attenuation between these sources has no significant effect on the data. The typical systematic uncertainty is  $\sim 10\%$  for NRO45. The typical systematic uncertainty of NMA is  $\sim 15\%$  because the primary flux-scale calibrators are not near to Cyg X-3 and phase noise caused by atmospheric fluctuations. Although flux loss due to pointing errors is corrected by pointing offset data in the data reduction process, the uncertainty of YT32 is as much as  $\sim 20\%$ . However, the relative uncertainties of flux density in a day should be much better than these values.

## 2.2. JVN observation

A follow-up VLBI observation was carried out with the Japanese VLBI Network (JVN; Fujisawa et al. 2007; Doi et al. 2006a; Doi et al. 2006b). The duration of the observation was from MJD= 53770.8 to MJD= 53771.4, i.e., starting 2.6 days after the first rise of the flare. The telescopes participating in this observation are four 20-m telescopes of the VLBI Exploration of Radio Astrometry project (VERA; Kobayashi et al. 2003), Usuda 64-m (U64), Kashima 34-m (K34), YT32, and Gifu 11-m (G11). Right-circular polarization was received at 8400–8416 MHz (IF1) and 8432–8448 MHz (IF2) with a total bandwidth of 32 MHz. The VSOP/K4-terminal system was used as a digital back-end; digitized data in 2-bit quantization are recorded onto magnetic tapes at a data rate of 128 Mbps. Two sources (2000+472, 3C454.3) other than Cyg X-3 were observed for gain and bandpass calibration, respectively. The data were correlated with the VSOP-FX correlator at NAOJ (Shibata et al. 1998), and fringe were detected at all baselines except for baselines including Ishigaki, Ogasawara, and G11 telescopes.

The data was reduced in the standard manner with the Astronomical Image Processing System (AIPS; Greisen 2003) developed at the US National Radio Astronomy Observatory. An amplitude-scaling factor was determined from monitored system noise temperatures and antenna efficiencies of U64, YT32, and K34 telescopes. Furthermore, we calibrated antenna gain variations using the data of 2000+472, which is a point source in the JVN baselines and scanned every 30–60 minutes. Such a calibration method provides an absolute flux scale with an accuracy of  $\sim 10\%$  and a relative time variation of antenna gain of  $\sim 3\%$  accuracy.

### 3. Results

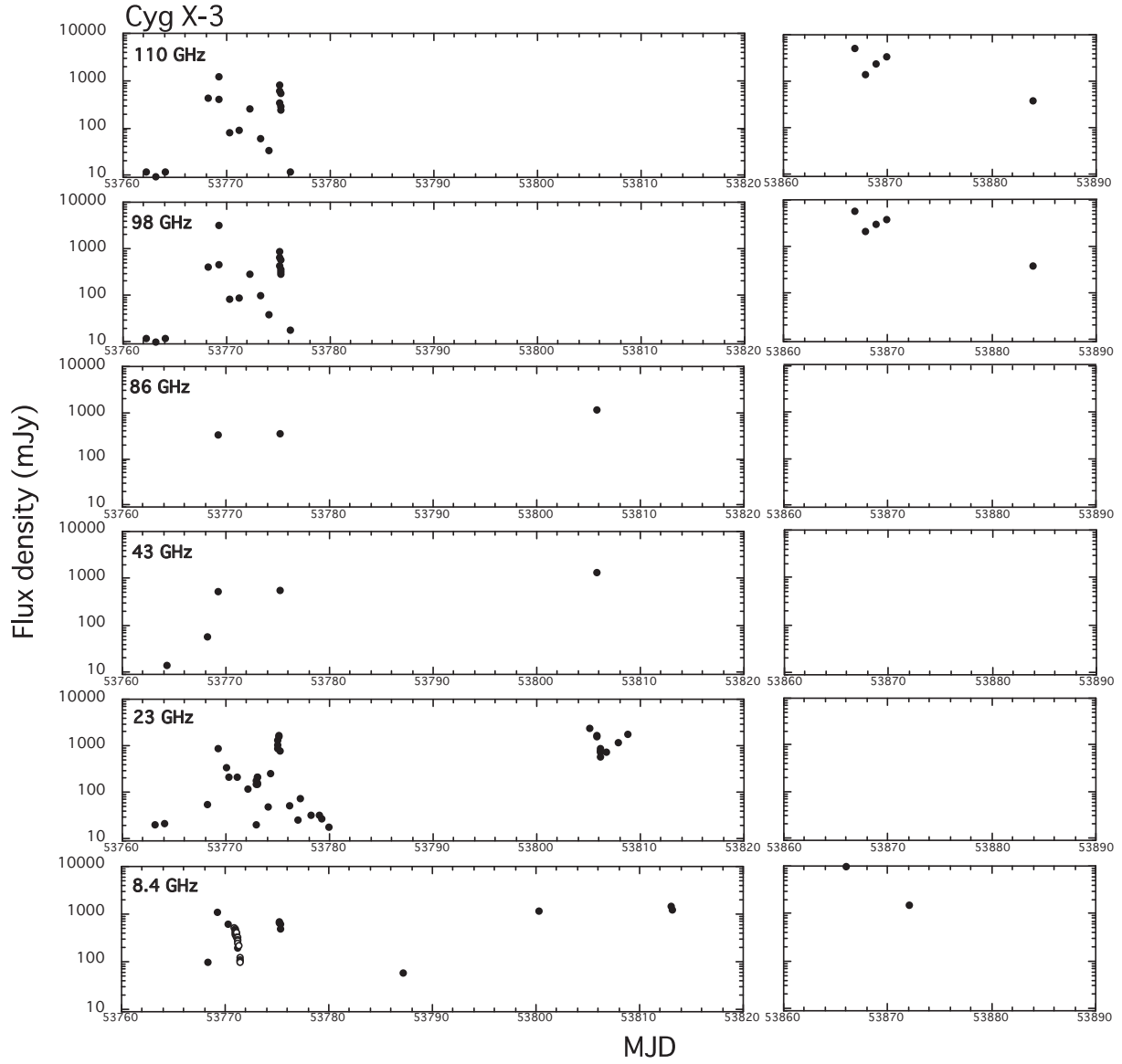
#### 3.1. Light curves

We present the light curves of Cyg X-3 at 6 frequency bands of 8.4, 23, 43, 86, 98, and 110 GHz obtained with NRO45, NMA, and YT32 in Fig. 1. Table 1 summarizes results of observations. The first rise of the flare was detected with NMA at MJD= 53768.13 or 3 am on February 2 2006 (UT) at 98 and 110 GHz. This is about 18 days after it entered the quenched state observed with RATAN-600. The first rise was also observed at lower frequencies within 1 day. After that, we observed several peaks exceeding 1 Jy. Although there is a long intermission of observation in our campaign, the duration of the active phase of Cyg X-3 is at least over 40 days (Tosaki et al. 2006). It can be confirmed that Cyg X-3 was still active in May from the flux densities at 8.4, 98, and 110 GHz in 2006 May in Fig. 1 and Table 1.

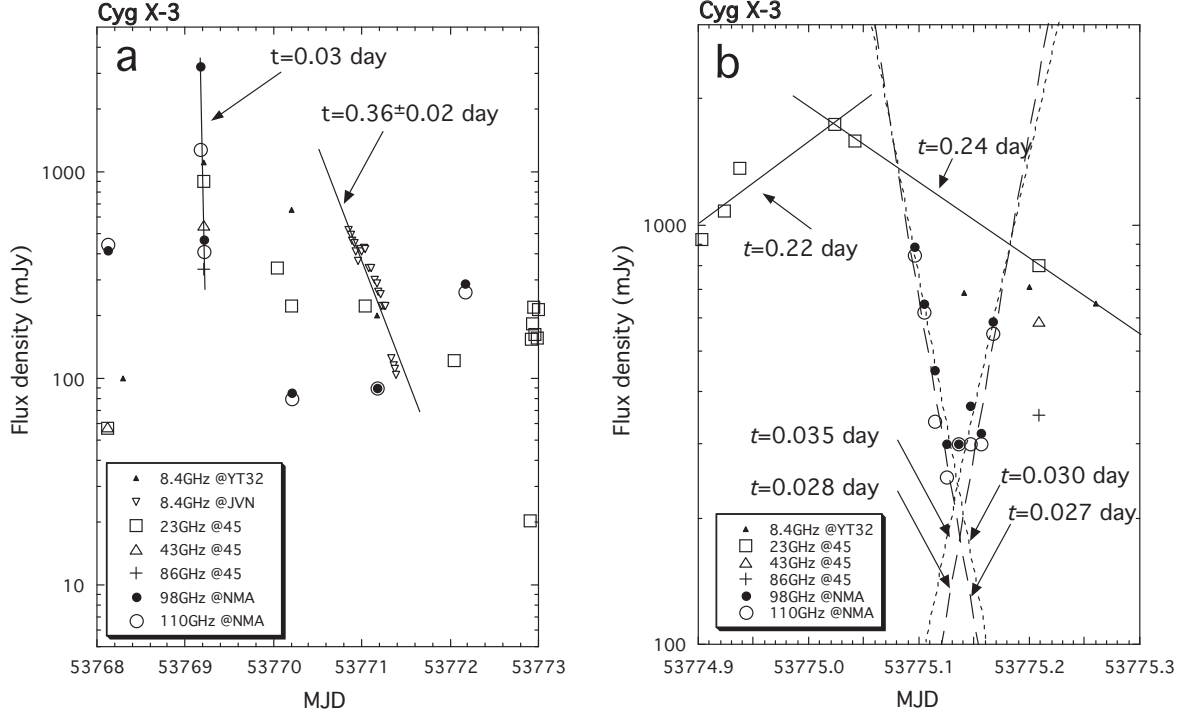
Figure 2a shows the enlarged light curves of the initial phase of the first flare. Before the flare, the flux density of Cyg X-3 was inhibited up to a few 10 mJy at 23 to 110 GHz (see Figure 1). At MJD= 53768.13, the first rise was found by NMA at 98 and 110 GHz, of which the flux densities became 40 times or more compared with the value of the previous day. The flux densities at 23 and 43 GHz with NRO45 were also 3-4 times brighter than the previous values. The peak flux densities at MJD= 53769.17 exceed 3 Jy at 98 GHz and 1 Jy at 110 GHz. They were violently variable and decreased to 1 Jy or less within one hour. Assuming an exponential decay, the e-folding decay times would be 0.03 days both at 98 GHz and 110 GHz. On the other hand, the e-folding decay time at 8.4 GHz are  $t = 0.36 \pm 0.02$  day during MJD= 53770 to 53771, which will be mentioned for details. For several major flares of Cyg X-3 observed previously, the e-folding decay time of the flux density was reported to be in the range of 0.15 to 2.75 days (Hjellming et al. 1974). The observed decay times are much shorter than these previous values.

Figure 2b shows the enlarged light curves of the second flare. We obtained a higher sampling rate light curve at 23 GHz in the rising phase of the second flare. At MJD= 53774.9, the rise of the second flare was detected at 23 GHz with the NRO45. The flux density at 23 GHz increased rapidly from 0.9 to 1.7 Jy within 3 hours. That corresponds to an e-folding rise time of  $t = 0.22 \pm 0.05$  day. The flux density decreased rapidly from the peak to 0.8 Jy by the next observation 4.4 hours after. If these flux densities are involved in the same flare, the e-folding decay time is  $t = 0.24 \pm 0.01$  day. The decay phase of the flare was also observed at other frequencies. The flux densities observed at 98 and 110 GHz decreased rapidly within the observation interval as at 23 GHz. A power law describes the decay behavior. The e-folding decay times at 98 and 110 GHz are  $t = 0.030 \pm 0.003$  day and  $t = 0.027 \pm 0.005$  day, respectively. These are of the same order of the first flare at 98 and 110 GHz. In addition to the peak and following decay at 23 GHz, another rising is recognized at 98 and 110 GHz in the observation break at 23 GHz. The e-folding rise times at 98 and 110 GHz are  $t = 0.035 \pm 0.025$  day and





**Fig. 1.** Radio light curves of February to May 2006 of Cygnus X-3 at, from bottom to top, 8.4, 23, 43, 86, 98, and 110 GHz. The 8.4 GHz data were obtained with YT32. In addition, open circles at 8.4 GHz show high-density sampling flux densities observed by the Japanese VLBI Network (JVN). The 23, 43 and 86 GHz data were obtained with NRO45. The 98 and 110 GHz data were obtained with NMA. The first rise was detected at MJD= 53768.13 at 98 and 110 GHz. Within one day after the first rise, the flux density at 23 GHz also increased. The 8.4, 98, and 110 GHz data show Cyg X-3 was in an active phase in May 2006.



**Fig. 2.** Enlarged radio light curves of Cyg X-3 at the first and second flares. **(a)** Observation epoch is from MJD = 53768 to 53773. At MJD= 53768.13, the first rise was found by NMA at 98 and 110 GHz, and the flux densities increased up to 0.4 Jy. This is 40 times or more compared with the value before the first rise. The flux densities at MJD= 53769.17 exceed 3 Jy at 98 GHz and 1 Jy at 110 GHz. They decreased to 1 Jy or less within one hour. The best-fitting curves of exponential decay model are plotted in lines. Open upside-down triangles show flux densities at 8.4 GHz observed by the Japanese VLBI Network (JVN). The flux densities at lower frequencies changed more gradually. **(b)** Observation epoch is from MJD = 53774.9 to 53775.3. Data with NMA at 98 and 110 GHz show clearly the quench and the successive rapid rise of the millimeter flux. The best-fit curves of exponential rise and decay models are plotted in lines. The e-folding rise and decay times are  $t \simeq 0.03$  day both at 98 and 110 GHz.

$t = 0.028 \pm 0.013$  day, respectively. The e-folding rise times are also at the same level as the decay times.

Figure 3 shows the relation between the time scale of the flux variability and frequency in the 2006 flares of Cyg X-3. The e-folding rise and decay times are derived from neighboring observations within 8 hours. Our data with higher sampling rates than previous reports should reveal new information about the synchrotron jets of Cyg X-3. The e-folding time is shorter at higher frequencies, and we fit the trend with a power-law model, shown as a straight line in the figure. Although the scattering of the data points is large, the e-folding time is inversely proportional to the observed frequency,  $T = 3.8f^{-1.03}$ . That cannot be explained in terms of the synchrotron bubble model, which predicts the same time scale for all the frequencies. It is suggested that the injection and loss of energy of relativistic electrons in the jet plays an important role in the spectral evolution of the flares of Cyg X-3.

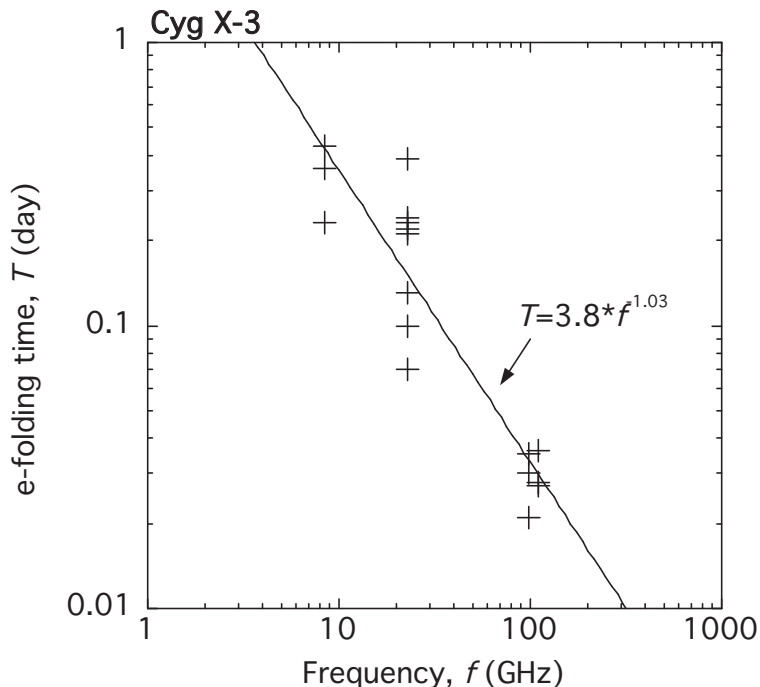


**Fig. 3.** The relation between the time scale of the flux variability and frequency in the 2006 flares of Cyg X-3. The solid line is the best-fitting power-law model for these data. The e-folding time of the flux variability should inversely relate frequency.

### 3.2. Spectral Evolution of Flares

Fig. 4 shows spectral evolution in the three days around the first flare of Cyg X-3. The curve in panel **a** indicates the spectrum at MJD= 53768.13, at the onset of the first flare. The rapid increase at 98 and 110 GHz takes place first as mentioned in the previous subsection, while the flux densities at lower frequencies do not change significantly. The spectrum shows a complicated inverted feature from 43 to 98 GHz. This suggests there is time lag of flare onset depending on frequency. The data in panel **b** indicate flux densities at 98 and 110 GHz at MJD= 53769.17. The flux densities at 98 GHz and 110 GHz rise to 3.2 and 1.3 Jy, respectively. These are the highest values in this flare. Unfortunately, no simultaneous data at other frequencies are available. Panel **c** shows the flux densities of Cyg X-3 at MJD= 53769.21, just after 1 hour of panel **b**. The flux densities at lower frequencies increased about 10 times over values in panel **a**, but flux densities at 98 and 110 GHz decreased dramatically in 1 hour. Then the spectrum is described by a power law with an index of  $\alpha \simeq -0.4$ . The peak flux is followed by a rapid decay at high frequency. Panel **d** shows the spectrum at MJD= 53770.21, or 1 day after the peak. The spectrum is also describable by a power law, but it was decayed to be as steep as  $\alpha \simeq -0.8$ . This is consistent with the decay time being shorter at higher frequency, as mentioned in the previous subsection. We assume that the spectral break seen at  $\sim 100$  GHz at MJD= 53768.13 moves in the spectrum down to below 8 GHz in one day. This evolution of the radio spectrum may be interpreted as the result of an adiabatic expansion of

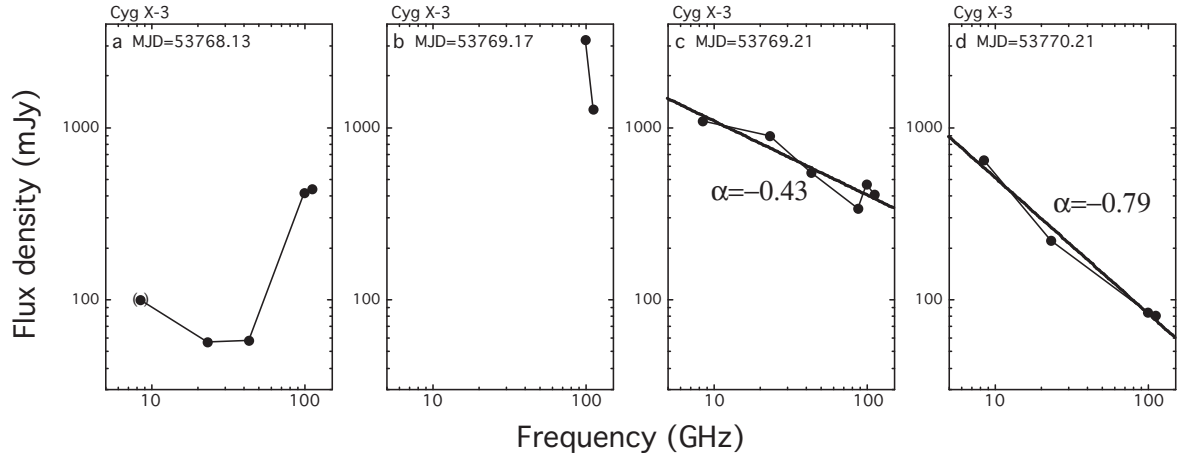


**Fig. 4.** Spectral evolution during the first flare. Three days evolution around the first peak at MJD= 53768. **a** On the first day at the first flare, MJD= 53768.14, the flux densities at 98 and 110 GHz increase rapidly, while the flux densities at lower frequencies were still low. **b** 98 and 110 GHz data at MJD= 53769.17. The flux densities at 98 GHz and 110 GHz were 3.2 and 1.3 Jy, respectively. These are the highest values in this flare. Unfortunately, it was not observed during this time at other frequencies. **c** Flux densities after 1 hour of panel **b**. The flux densities at 8.4, 22, and 43 GHz increased about 10 times over values in panel **a**. Flux densities at 98 and 110 GHz decreased dramatically in 1 hour. A power-law model,  $S \propto f^\alpha$ , is applied to these (solid line). The best fitting of the spectral index is  $\alpha \simeq -0.4$ . **d** Flux densities after 1 day of panel **c**. Although the flux densities were described by a power law (solid line), the spectrum was fairly steepened. The best fitting of the spectral index is  $\alpha \simeq -0.8$ .

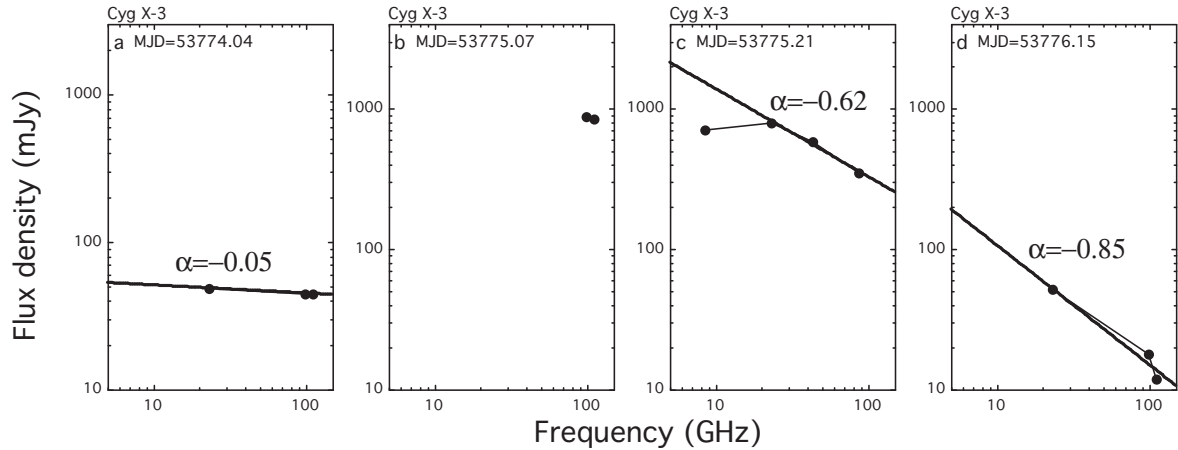


**Fig. 5.** Three days spectral evolution during the second flare around MJD= 53775. **a** Flux densities one day before the second flare, or at MJD= 53774.04. The flux densities were described by a power law with  $\alpha \simeq -0.1$  (solid line). **b** Flux densities at MJD= 53775.07. These are the highest values at 98 and 110 GHz in this flare. They would be near the peak of this flare because the highest value appeared at 22 GHz before 1 hour. Unfortunately, it was not observed during this time at 98 and 110 GHz. **c** Flux densities after 3 hour of panel **b**, Between these two panels, Cyg X-3 decreased and increased rapidly. (see also Fig 2b). Flux densities except for at 8.4 GHz were described by a power law with  $\alpha \simeq -0.6$  (solid line). **d** Flux densities after 1 day of panel **c**. The spectrum was steepened. The best fitting of the spectral index is  $\alpha \simeq -0.8$ .

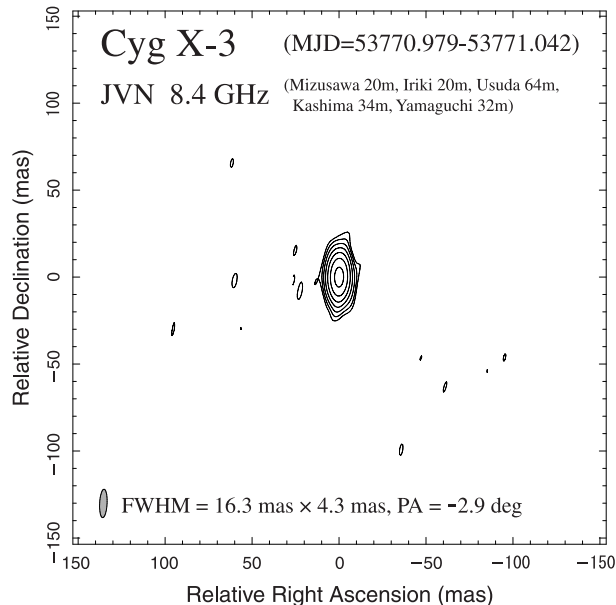
synchrotron emitting ejecta in Cyg X-3.

Figure 5 shows the spectral evolution in the three days around the second flare. Panel **a** in this figure indicates spectra on the day before the second peak or at MJD= 53774.04. This shows a flat spectrum with an index of  $-0.1$ , which suggests that the second flare has already started. The spectrum at another flare in March was also flat over the observation band, suggesting an optically thick radio source. A power law with an index of  $-0.2$  can explain the spectrum. Panel **b** shows flux densities at MJD= 53775.07. These are the highest values at 98 and 110 GHz in this flare. Following this, these decreased rapidly. However, they would be near the peak of this flare, because the value at 22 GHz reached the maximum before 1 hour. Unfortunately, it was not observed during this time at 98 and 110 GHz. Panel **c** shows flux densities after 3 hour of panel **b**, Between these two panels, Cyg X-3 decreased and increased rapidly. (see also Fig 2b). Flux densities except for at 8.4 GHz were described by a power law with  $\alpha \simeq -0.6$  (solid line). The spectral index is slightly steeper than that in the corresponding phase of the first flare. And panel **d** shows flux densities after 1 day of panel **c**. The spectrum was steepened. The best fitting of the spectral index is  $\alpha \simeq -0.9$ . The spectral index of  $-0.9$  is similar to that one day after the first flare. The decay time of the second flare is also shorter at higher frequencies, which cannot be explained by the sole synchrotron bubble model.

### 3.3. 8.4 GHz VLBI results in a flare

Our VLBI observation started from just 2 days after the first rise of the flare, i.e., the first day after the intensity maximum of the first flare. Successive snapshots with a short integration time have been made because rapid flux decrease has also been observed during the VLBI observation. Fig. 6 is an example of such a snapshot, of which observation period is from MJD= 53770.979 to 53771.042. Only a featureless (extended) structure is found in all snapshot images. Deconvolution with the structure model of an elliptical Gaussian profile and self-calibration was done using DIFMAP software (Shepherd 1997). The deconvolved source size was  $\sim 8$  mas. This is significantly broader than a synthesized beam size,  $16.3 \text{ mas} \times 4.3 \text{ mas}$  at PA of  $-2.9^\circ$ . However, no other component is found beyond three times the r.m.s. of noise of the resultant image or a brightness temperature of  $7.5 \times 10^5$  K.

We also analyzed the time evolution of flux density and source structure during the JVN observation. We have clipped out a series of data segments. Each segment has a duration of 1 hour, and the interval of the starting time of the segments is set to be 0.5 hour, i.e., half of a duration overlapping the half of the next duration. Using the task of UVFIT in AIPS, we measured a source size and a flux density for each clipped data by visibility-based model-fitting using an elliptical Gaussian profile model. The flux density of the component decreased from  $\sim 500$  mJy to  $\sim 100$  mJy during the VLBI observation lasting  $\sim 14$  hours (Fig.2a and Fig 7a). The source structure has hardly changed, regardless of the variability of the synthesized beam (Fig.7b and 7c). The weighted averages of major axis, minor axis, and position angles of the



**Fig. 6.** Snapshot image of Cyg X-3 from VLBI data in MJD = 53770.979 to 53771.042 (1.5 hour). The beam size is  $16.3 \text{ mas} \times 4.3 \text{ mas}$  at PA of  $-2.9^\circ$ , corresponding to  $157 \text{ AU} \times 41 \text{ AU}$  at the distance to Cyg X-3. R.M.S. of image noise,  $\sigma$ , is  $0.70 \text{ mJy beam}^{-1}$ . Contour levels are  $3\sigma \times (-1, 1, 2, 4, 8, 16, 32, 64)$ .

source structure are  $8.9 \pm 0.1 \text{ mas}$ ,  $7.1 \pm 0.1 \text{ mas}$ , and  $15.0 \pm 2.3 \text{ deg}$ , respectively, i.e., we have resolved the source which is slightly but significantly elongated in a north-south direction. Our VLBI observation has revealed that Cyg X-3 has no significant structure change in spite of the rapid flux variability at 8.4 GHz during the period.

Previous studies (Miller-Jones et al. 2004) show that the two-sided jets are ejected toward north and south after major radio flares. If the ejection was concurrent with the first rise of the flux and the jet axis is fairly close to perpendicular to the line of sight, the traveling distance of the ejecta is expected to be 350 AU or 35 mas at 10 kpc. However, we have not found any evidence of such a jet structure. The source size in our VLBI image is presumably affected by interstellar scattering because it is consistent with the expected scattering size at 8.4 GHz (Schalinski et al. 1995). Thus, there is no structural evolution on a scale of larger than 5 mas in spite of rapid flux variability. That may be a strong constraint on jet evolution in a few days after a radio flare.

The authors would like to thank the members of NRO45 group and NMA group of Nobeyama Radio Observatory for support in the observations. This work is partially supported by the Japan-Russia Research Cooperative Program of Japan Society for the Promotion of Science. The studies are partially supported by the Russian Foundation Base Research (RFBR) grant N 05-02-17556 and the mutual RFBR and Japan Society for the Promotion of Science (JSPS) grant N 05-02-19710. The JVN project is led by the National Astronomical Observatory of Japan (NAOJ) that is a branch of the National Institutes of

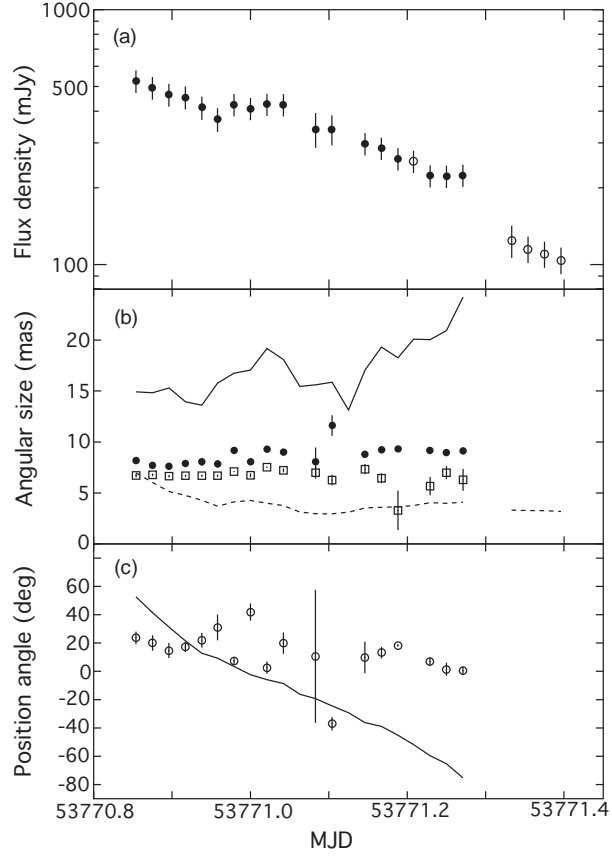


**Fig. 7.** Evolution of source structure of Cyg X-3 obtained with VLBI. A series of measurements were performed by visibility-based model-fitting using an elliptical-Gaussian profile model with free parameters of flux density, major and minor axes of FWHM, and position angle of the major axis (see text in detail). **(a)** Flux densities of VLBI component (filled circle). Open circles represent measurements using a circular-Gaussian model, rather than elliptical one, due to poor data quality. **(b)** Angular sizes of fitted source structure. Filled circles and open squares represent the FWHMs of major and minor axes, respectively. Solid and dashed lines represent the major and minor axes of HPBWs of synthesized beam in uniform-weighting, for comparison. **(c)** Position angles of major axis of fitted source structure (open circle). Solid line represents the position angle of the major axis of synthesized beam, for comparison.



Natural Sciences (NINS), Hokkaido University, Gifu University, Yamaguchi University, and Kagoshima University, in cooperation with the Geographical Survey Institute (GSI), the Japan Aerospace Exploration Agency (JAXA), and the National Institute of Information and Communications Technology (NICT). TK is supported by a 21st Century COE Program at Tokyo Tech “Nanometer-Scale Quantum Physics” by the Ministry of Education, Culture, Sports, Science and Technology.

## References

- Braes, L. L. E., & Miley, G. K. 1972, *Nature*, 237, 506
- Doi, A., et al. 2006a, astro-ph/0612528
- Doi, A., et al. 2006b, *PASJ*, 58, 777
- Fujisawa, K., et al. 2007, in prep.
- Gregory, P. C., Kronberg, P. P., Seaquist, E. R., Hughes, V., A., Woodsworth, A., Viner, M. R., & Retallack, D. 1972, *Nature*, 239, 440
- Hjellming, R. M., Brown, R. L., & Blankenship, L. C. 1974, *ApJ*, 194, L13
- Hjellming, R. M., & Johnston, K. J. 1988, *ApJ*, 328, 600
- Kobayashi, H., et al. 2003, *Astronomical Society of the Pacific Conference Series*, 306, 367
- Greisen, E. W. 2003, *Information Handling in Astronomy - Historical Vistas*, 109
- McCullough, M. L., Robinson, C. R., Zhang, S. N., Harmon, B. A., Hjellming, R. M., Waltman, E. B., Foster, R. S., Ghigo, F. D., Briggs, M. S., Pendleton, G. N., & Johnston, K. J. 1999, *ApJ*, 517, 951
- Miller-Jones, J. C. A., Blundell, K. M., Rupen, M. P., Mioduszewski, A. J., Duffy, P., & Beasley, A. J. 2004, *ApJ*, 600, 368
- Okumura, S. K., Momose, M., Kawaguchi, N. et al., 2000, *PASJ*, 52, 393
- Ott, M., Witzel, A., Quirrenbach, A., et al., 1994, *A&A* 284, 331
- Predehl, P., Bruwitz, V., Paerels, F., & Trümper, J. 2000, *A&A*, 357, L25
- Schalinski, C. J., et al. 1995, *ApJ*, 447, 752
- Schalinski, C. J., Johnston, K. J., Witzel, A., Waltman, E. B., Umana, G., Pavelin, P. E., Ghigo, F. D., Venturi, T., Mantovani, F., Foley, A. R., Spencer, R. E., & Davis, R. J. 1998, *A&A*, 329, 504
- Shepherd, M. C. 1997, *ASP Conf. Ser. 125: Astronomical Data Analysis Software and Systems VI*, 125, 77
- Shibata, K. M., Kameno, S., Inoue, M., & Kobayashi, H. 1998, *ASP Conf. Ser. 144: IAU Colloq. 164: Radio Emission from Galactic and Extragalactic Compact Sources*, 144, 413
- Trushkin, S. A., Nizhelskij, N. A., Bursov, N. N., & Majorova, E. K. 2006, in *IAU Symp. 238*, 166
- Tsuboi, M. et al. 2006, *ATel*, 727, 1
- Tosaki, T., Tsuboi, M., Nakanishi, K., Trushkin, S., Fujisawa, K., Kameya, O., Kotani, T., & Kawai, N. 2006, *ATel*, 952, 1
- Tsutsumi, T., Morita, K.-I., & Umeyama, S. 1997, in *ASP Conf. Ser. 125, Astronomical Data Analysis Software and Systems VI*, ed. G. Hunt & H. E. Payne (San Francisco: ASP), 50

Waltman, E. B., Fiedler, R. L., Johnston, K. L., & Ghigo, F. D. 1994, AJ, 108, 179

**Table 1.** Flux densities of Cyg X-3

MJD	$S_{8.4}$ GHz	$S_{23}$ GHz	$S_{43}$ GHz	$S_{86}$ GHz	$S_{98}$ GHz	$S_{110}$ GHz
[day]	[mJy]	[mJy]	[mJy]	[mJy]	[mJy]	[mJy]
53762.181					12	12
53763.125		20			10	9.6
53764.083		21			12	12
53764.208			15			
53768.125		57	58		417	442
53768.292	100					
53769.167					3247	1280
53769.208	1100	896	549	338	468	408
53770.042		339				
53770.208	650	222			85	80
53771.042		224				
53771.167	200				89	90
53772.042		122				
53772.167					288	260
53772.910		20				
53772.924		155				
53772.934		183				
53772.951		219				
53772.965		163				
53772.982		156				
53772.995		214				
53773.208					104	60
53774.042		49			39	35
53774.208		255				
53774.903		922				
53774.924		1080				
53774.937		1365				
53775.024		1732				
53775.042		1589				
53775.096					890	850
53775.104					650	620
53775.115					450	340
53775.125					300	250
53775.135					300	300

Table 1. (Continued.)

MJD [ <i>day</i> ]	$S_{8.4}$ GHz [ <i>mJy</i> ]	$S_{23}$ GHz [ <i>mJy</i> ]	$S_{43}$ GHz [ <i>mJy</i> ]	$S_{86}$ GHz [ <i>mJy</i> ]	$S_{98}$ GHz [ <i>mJy</i> ]	$S_{110}$ GHz [ <i>mJy</i> ]
53775.140	690					
53775.146					370	300
53775.156					320	300
53775.167					590	550
53775.200	710					
53775.208		801	587	352		
53775.260	650					
53775.320	500					
53776.152		52			18	12
53776.958		25				
53777.188		74				
53778.208		33				
53778.948		34				
53779.208		29				
53779.937		18				
53787.125	60					
53800.208	1200					
53805.118		2424				
53805.729		1762				
53805.750		1609				
53805.757			1402	1203		
53806.090		805				
53806.104		896				
53806.118		733				
53806.139		601				
53806.708		764				
53807.771		1192				
53808.771		1782				
53813.000	1530					
53813.083	1260					
53866.014	10000					
53866.847					6000	5200
53867.847					2200	1400
53868.847					3000	2500
53869.847					3900	3500

Table 1. (Continued.)

MJD	$S_{8.4}$ GHz	$S_{23}$ GHz	$S_{43}$ GHz	$S_{86}$ GHz	$S_{98}$ GHz	$S_{110}$ GHz
[ <i>day</i> ]	[ <i>mJy</i> ]	[ <i>mJy</i> ]	[ <i>mJy</i> ]	[ <i>mJy</i> ]	[ <i>mJy</i> ]	[ <i>mJy</i> ]
53872.014	1500					
53883.847					400	400